J. Fluid Mech. (1970), *vol.* 40, *part* 2, *pp.* 225–239
Printed in Great Britain

The spin-up of a homogeneous fluid bounded below by a permeable medium

By JOHN KROLL
Department of Engineering and Applied Science, Yale University
AND GEORGE VERONIS
Department of Geology and Geophysics, Yale University

(Received 5 June 1969)

The spin-up of a homogeneous rotating fluid bounded at the top and/or bottom by a permeable medium has been proposed by Bretherton & Spiegel (1968) as a model for the spin-up in natural flows where turbulent processes transmit the direct effect of the boundaries deeper into the fluid than does the laminar Ekman layer. The theoretical analysis for the spin-up of a laterally unbounded fluid bounded by a permeable medium below is presented here. In addition, an experimental study of the process is presented. Theory and experiment agree reasonably well with a maximum difference of about 8% in the predicted and measured spin-up times. The effects of the side-wall boundary have been studied theoretically by Howard (1969). Experimental observations in the side-wall boundary layer confirm qualitatively the results of Howard's theory.

1. Introduction

Consider a cylinder filled with a fluid and rotating about its axis with uniform angular velocity $\Omega - \Delta\Omega$. If at time $t = 0$ the angular velocity of the cylinder is increased to Ω, the fluid in the immediate vicinity of the boundary will feel the change immediately, but the bulk of the fluid will continue to rotate with angular velocity $\Omega - \Delta\Omega$. The process by which the fluid achieves the new rotation rate, Ω, has been described by Greenspan & Howard (1963). This so-called spin-up takes place as follows:

In a period of time of the order of Ω^{-1}, Ekman boundary layers at the top and bottom of the cylinder are established. Within these layers, the fluid feels the new rotation rate, and is thrown outward by the increased centrifugal force. The outgoing fluid in the boundary layer is replaced by a vertical flow of fluid into the boundary layers from the interior. This vertical flow is accompanied by a radially inward flux of fluid in the interior and, since viscous effects are not significant in the interior, the conservation of angular momentum requires that the inward flowing particles increase their angular velocity. This secondary flow constitutes the spin-up of the interior fluid.

For a container with rigid boundaries the rapidity of the spin-up process depends on the rate at which the Ekman boundary layers suck fluid from the interior. If the solid boundaries at the top and bottom of the container are

replaced by permeable boundaries, the vertical flux from the interior can be increased and, since the permeable medium can impart the new rotation rate to the incoming fluid very effectively, the entire process can be speeded up. Bretherton & Spiegel (1968) suggested that in geophysical or astrophysical flows the mixed layers near the surface can be simulated by a permeable medium, which could enhance the spin-up process. In his famous paper on wind-driven currents, Ekman (1905) assumed an eddy coefficient of viscosity for the surface regions of the ocean and thereby incorporated the same effect.

The present paper treats the spin-up of a fluid bounded above and below by a permeable medium. The theoretical analysis is given in §2. We make liberal use of the ideas introduced by Greenspan & Howard and described in Greenspan's (1968) book. In particular, the time scale of the flow is assumed to be of the order of the spin-up time for the problem with solid boundaries. The effect of the permeable medium is introduced by matching the appropriate variables of the free fluid to those of the permeable medium, evaluated at the boundary interface.

The resulting spin-up time follows by means of a straightforward analysis, and it has the value

$$T = \frac{1}{\Omega}\left[\frac{1+4N^2}{(4Nh/L)+2NE^{\frac{1}{2}}+E^{\frac{1}{2}}}\right],$$

where $N = k\Omega/\nu$, k is the permeability, ν is the kinematic viscosity, E is the Ekman number, h is the depth of the permeable medium, and L is the half depth of the fluid. As $N \to 0$, so that the boundary becomes impermeable, the ordinary spin-up time of Greenspan & Howard is recovered, and as $N \to \infty$ the limiting behaviour is the cylindrical counterpart of that deduced by Bretherton & Spiegel for a sphere, where the Ekman layers are unimportant. For the geophysical or astrophysical situations, in which the permeable medium serves as the analogue to the convectively unstable surface layers, the latter extreme is appropriate.

The experimental arrangement for the observation of the spin-up time is straightforward, and is described in §3. The spin-up time was determined by photographing from above the position of a straight line of dye which was generated before the tank was spun up. In §4, we compare these experimental results with the theory. The comparison is quite good, with agreement within 8 % for each run.

In our analysis we omitted the effects of the side-wall boundary layer. These effects are the subject of a study by Howard (1969). As described in §5, we observed the structure of the azimuthal velocity profile from both the vertical and the horizontal, and compared the observations with Howard's theoretical results for the lateral boundary layer. Howard analyzed cases where the parameter $\beta = (\nu T/h^2)^{\frac{1}{2}}$ was large or small. In our experiments, we examined flows where β was small, which implied that the spin-up time T was much less than the characteristic diffusion time h^2/ν, based on the thickness h of the permeable medium.

For small β, Howard predicts that in the boundary layer there will be a large backward displacement in the azimuthal direction in addition to the backward displacement in the interior. The physical reason for this is that the fluid in the permeable medium senses the wall at a distance from it of the order of the depth,

h, begins to slow down, and is forced up into the essentially inviscid interior. The result is that the fluid in the interior spins down in this region causing the backward displacement. A more detailed description of the physical process is presented in §5. We were able to observe the qualitative behaviour predicted by Howard, but not the magnitude of the effect. The reason for this is that we were not able to generate a flow in which the Stewartson layer of thickness $LE^{\frac{1}{4}}$ is much thinner than Howard's boundary layer, a condition which Howard assumed in his development.

There exists a point in the fluid within the side boundary layer, where the final position in the vertical direction remains unchanged after spin-up is complete. We measured the distance of this point from the side wall, and found it to be in reasonably good agreement with Howard's theory.

2. Theoretical analysis

Consider the cylindrical configuration shown in figure 1. Initially the fluid is spinning with solid body rotation Ω_0. Then the cylinder is spun up by an amount $\Delta\Omega$. After an amount of time, characterized by the spin-up time T, the fluid

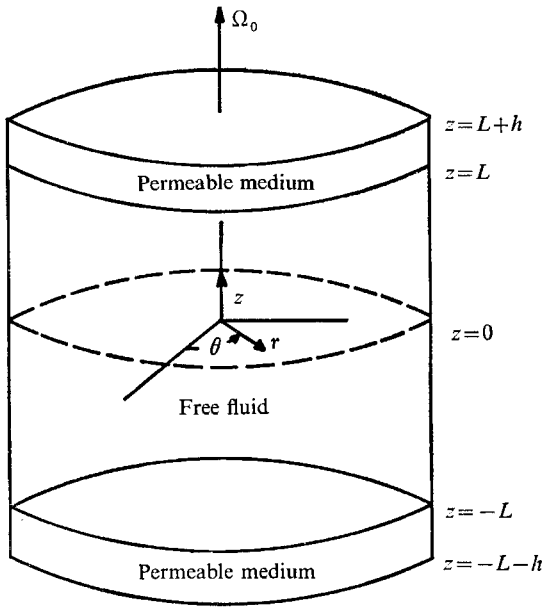

FIGURE 1. The geometrical configuration of the problem.

reaches solid body rotation at the final value $\Omega = \Omega_0 + \Delta\Omega$. As in the ordinary spin-up problem, the effects of the side wall can be neglected in determining the spin-up time, because the spin-up time will be so much smaller than the diffusion time.

There are two flow régimes to consider, the free fluid and the flow of the fluid in the permeable medium. Solutions of the flow field in each of the régimes can

be found, and the solutions matched at the interface between the fluid and the permeable medium.

Equations describing the free fluid are the Navier–Stokes equations for a rotating fluid and the continuity equation. These equations in dimensionless form with the velocity $\mathbf{V}$, measured with respect to the final rotation rate Ω, are

$$\frac{\partial \mathbf{V}}{\partial t} + \epsilon \mathbf{V} \cdot \nabla \mathbf{V} + 2\hat{\mathbf{k}} \times \mathbf{V} = -\nabla P + E\nabla^2 \mathbf{V}, \tag{1}$$

$$\nabla \cdot \mathbf{V} = 0, \tag{2}$$

where $\epsilon (= \Delta\Omega/\Omega)$ is the Rossby number, $E (= \nu/L^2\Omega)$ is the Ekman number, and $\hat{\mathbf{k}}$ is the unit vector in the z-direction. The centrifugal and gravitational body force terms are absorbed in P. For these equations, time is non-dimensionalized by Ω^{-1}, length by L, velocity by $\Delta\Omega L$, and pressure by $\rho L\Omega(\Delta\Omega L)$.

The equations describing the flow in the permeable medium are Darcy's law and the continuity equation.

Darcy's law in dimensional variables is

$$\mathbf{V} = -\frac{k}{\mu}(\nabla p - \mathbf{F}), \tag{3}$$

where $\mathbf{F}$ is the sum of applied body forces and k is the permeability of the medium. From the assumption that the fluid in the permeable medium reaches Ω instantaneously in comparison to the spin-up time, $\mathbf{F}$ will consist of the gravitational force, and the centrifugal and Coriolis forces due to the rotation $\boldsymbol{\Omega}$.

$$\mathbf{F} = -\rho\boldsymbol{\Omega} \times (\boldsymbol{\Omega} \times \mathbf{r}) - \rho 2\boldsymbol{\Omega} \times \mathbf{V} - \rho g\hat{\mathbf{k}}. \tag{4}$$

Equations (3) and (4) can be non-dimensionalized in exactly the same manner as described above, which yields Darcy's law in dimensionless form ($\boldsymbol{\Omega} = \hat{\mathbf{k}}\Omega$):

$$\mathbf{V} = -N(\nabla P + 2\hat{\mathbf{k}} \times \mathbf{V}), \tag{5}$$

where $N = k\Omega/\nu$ and, as before, the centrifugal and gravity forces are absorbed in P. The continuity equation for the permeable medium is the same as (2).

Since this problem is similar to the ordinary Ekman spin-up problem, we will assume some of the characteristic features of that problem to be true for this problem. So we will make the following assumptions:

(i) The Rossby number, $\epsilon = \Delta\Omega/\Omega$, is taken to be sufficiently small so that the problem is linear.

(ii) The variables in the free fluid can be divided into an interior part (denoted by subscript I) and a boundary layer part (denoted by an overbar). Thus,

$$\mathbf{V} = \mathbf{V}_I + \bar{\mathbf{V}}, \quad P = P_I + \bar{P}, \tag{6}$$

where $\bar{\mathbf{V}}$ decays to zero in the interior.

(iii) In the interior,

$$\frac{\partial}{\partial r} = O(1), \quad \frac{\partial}{\partial z} = O(1), \quad \text{and} \quad \frac{\partial}{\partial \theta} = 0 \tag{7}$$

because of azimuthal symmetry. In the boundary layers at $z = \pm 1$,

$$\frac{\partial}{\partial r} = O(1), \quad \frac{\partial}{\partial z} = \mp E^{-\frac{1}{2}} \frac{\partial}{\partial \zeta}, \quad \text{where} \quad \frac{\partial}{\partial \zeta} = O(1). \tag{8}$$

(iv) In both the interior and the boundary layers, the time scale is of the order $E^{-\frac{1}{2}}$. Thus,

$$\frac{\partial}{\partial t} = E^{\frac{1}{2}}\frac{\partial}{\partial \tau}, \quad \text{where} \quad \frac{\partial}{\partial \tau} = O(1). \tag{9}$$

With these assumptions, (1) and (2) for the free fluid take the following form for the interior,

$$E^{\frac{1}{2}}\frac{\partial u_I}{\partial \tau} - 2v_I = -\frac{\partial P_I}{\partial r} + E\left[\frac{\partial}{\partial r}\left(\frac{1}{r}\frac{\partial}{\partial r} r u_I\right) + \frac{\partial^2 u_I}{\partial z^2}\right], \tag{10a}$$

$$E^{\frac{1}{2}}\frac{\partial v_I}{\partial \tau} + 2u_I = E\left[\frac{\partial}{\partial r}\left(\frac{1}{r}\frac{\partial}{\partial r} r v_I\right) + \frac{\partial^2 v_I}{\partial z^2}\right], \tag{10b}$$

$$E^{\frac{1}{2}}\frac{\partial w_I}{\partial \tau} = -\frac{\partial P_I}{\partial z} + E\left[\frac{1}{r}\frac{\partial}{\partial r}\left(r\frac{\partial w_I}{\partial r}\right) + \frac{\partial^2 w_I}{\partial z^2}\right], \tag{10c}$$

$$\frac{1}{r}\frac{\partial}{\partial r}(r u_I) + \frac{\partial w_I}{\partial z} = 0. \tag{10d}$$

For the boundary layer at $z = -1$ (we consider only the bottom boundary layer, since the upper one can be treated in the same fashion):

$$E^{\frac{1}{2}}\frac{\partial \bar{u}}{\partial \tau} - 2\bar{v} = -\frac{\partial \bar{P}}{\partial r} + E\left[\frac{\partial}{\partial r}\left(\frac{1}{r}\frac{\partial}{\partial r} r\bar{u}\right)\right] + \frac{\partial^2 \bar{u}}{\partial \zeta^2}, \tag{11a}$$

$$E^{\frac{1}{2}}\frac{\partial \bar{v}}{\partial \tau} + 2\bar{u} = E\left[\frac{\partial}{\partial r}\left(\frac{1}{r}\frac{\partial}{\partial r} r\bar{v}\right)\right] + \frac{\partial^2 \bar{v}}{\partial \zeta^2}, \tag{11b}$$

$$E^{\frac{1}{2}}\frac{\partial \bar{w}}{\partial \tau} = -E^{-\frac{1}{2}}\frac{\partial \bar{P}}{\partial \zeta} + E\left[\frac{1}{r}\frac{\partial}{\partial r}\left(r\frac{\partial \bar{w}}{\partial r}\right)\right] + \frac{\partial^2 \bar{w}}{\partial \zeta^2}, \tag{11c}$$

$$\frac{1}{r}\frac{\partial}{\partial r}(r\bar{u}) + E^{-\frac{1}{2}}\frac{\partial \bar{w}}{\partial \zeta} = 0, \tag{11d}$$

where u is the radial velocity, v the azimuthal velocity and w the vertical velocity.

To solve the above equations, we will assume a series solution in powers of $E^{\frac{1}{2}}$, where $E^{\frac{1}{2}} \ll 1$. Thus,

$$(\mathbf{V}_I, \bar{\mathbf{V}}, P_I, \bar{P}) = \sum_{n=0}^{\infty} E^{\frac{1}{2}n}(\mathbf{V}_{In}, \bar{\mathbf{V}}_n, P_{In}, \bar{P}_n). \tag{12}$$

Then we use (12) in the sets of (10) and (11), and we equate the terms of like powers of $E^{\frac{1}{2}}$.

Thus we obtain, for the interior,

$$E^0\colon\ -2v_{I0} = -\frac{\partial P_{I0}}{\partial r}, \quad 2u_{I0} = 0, \quad 0 = \frac{\partial P_{I0}}{\partial z}, \tag{13a,b,c}$$

$$\frac{1}{r}\frac{\partial}{\partial r}(r u_{I0}) + \frac{\partial w_{I0}}{\partial z} = 0, \tag{13d}$$

where u_{I0} vanishes;

$$E^{\frac{1}{2}}: \; -2v_{I1} = -\frac{\partial P_{I1}}{\partial r}, \tag{14a}$$

$$\frac{\partial v_{I0}}{\partial \tau} + 2u_{I1} = 0, \tag{14b}$$

$$\frac{\partial w_{I0}}{\partial \tau} = -\frac{\partial P_{I1}}{\partial z}, \tag{14c}$$

$$\frac{1}{r}\frac{\partial}{\partial r}(ru_{I1}) + \frac{\partial w_{I1}}{\partial z} = 0. \tag{14d}$$

For the boundary layer, we obtain

$$E^{-\frac{1}{2}}: \; 0 = \frac{\partial \overline{P}_0}{\partial \zeta}, \quad \frac{\partial \overline{w}_0}{\partial \zeta} = 0; \tag{15a,b}$$

$$E^{0}: \; -2\overline{v}_0 = -\frac{\partial \overline{P}_0}{\partial r} + \frac{\partial^2 \overline{u}_0}{\partial \zeta^2}, \tag{16a}$$

$$2\overline{u}_0 = \frac{\partial^2 \overline{v}_0}{\partial \zeta^2}, \quad 0 = \frac{\partial \overline{P}_1}{\partial \zeta}, \tag{16b,c}$$

$$\frac{1}{r}\frac{\partial}{\partial r}(r\overline{u}_0) + \frac{\partial \overline{w}_1}{\partial \zeta} = 0. \tag{16d}$$

All boundary layer quantities must vanish as $\zeta \to \infty$. Thus, from (15a) and (15b), $\overline{P}_0 = \overline{w}_0 = 0$. Using the fact that $w = 0$ at $z = 0$, due to vertical symmetry, and that $\overline{w}_0 = 0$, we find from (13d) that $w_{I0} = 0$.

Now let us assume that the radial and azimuthal velocities have the following form in the free fluid and the permeable medium,

$$u = rU(z, \tau); \quad v = rV(z, \tau). \tag{17}$$

As in the analysis of Greenspan & Howard (1963), this form of solution works because we are neglecting side-wall effects, and have no characteristic radial dimension.

Equations (13a) and (13c) imply that V_{I0} is not a function of z. Combining (14b) and (14d), and using the assumption of (17), we derive

$$\frac{\partial V_{I0}(\tau)}{\partial \tau} = \frac{\partial w_{I1}(z, \tau)}{\partial z}. \tag{18}$$

Integrating (18) from $z = 0$ to $z = -1$, noting that $w_{I1} = 0$ at $z = 0$ because $w = 0$ and $\overline{w}_1 = 0$ at $z = 0$ (which corresponds to $\zeta = \infty$ in the boundary layer), yields

$$-\frac{\partial V_{I0}}{\partial \tau} = w_{I1}|_{z=-1}. \tag{19}$$

The Ekman layer equations (16a) and (16b) yield

$$\overline{u}_0 = re^{-\zeta}[A(\tau)\cos\zeta + B(\tau)\sin\zeta], \tag{20}$$

$$\overline{v}_0 = re^{-\zeta}[B(\tau)\cos\zeta - A(\tau)\sin\zeta], \tag{21}$$

where $A(\tau)$ and $B(\tau)$ are arbitrary functions of τ, which must be found from the boundary conditions. $\overline{w}_1$ can be found from (16*d*):

$$\overline{w}_1 = e^{-\zeta}[(A+B)\cos\zeta - (A-B)\sin\zeta]. \tag{22}$$

The following boundary conditions must be satisfied (subscript p stands for quantities in the permeable medium):

at $z = -1$,

$$(\text{B.C. } 1)\frac{\partial P}{\partial r} = \frac{\partial P_p}{\partial r}; \quad (\text{B.C. } 2)\, u = u_p; \quad (\text{B.C. } 3)\, v = v_p; \quad (\text{B.C. } 4)\, w = w_p;$$

at $z = -1-(h/L)$ ($z = -L-h$ dimensional),

$$(\text{B.C. } 5)\; w_p = 0.$$

For the permeable medium from (5),

$$u_p = -N\left[\frac{\partial P_p}{\partial r} - 2v_p\right], \tag{23}$$

$$v_p = -2Nu_p, \tag{24}$$

$$w_p = -N\frac{\partial P_p}{\partial z}. \tag{25}$$

From continuity,

$$\frac{1}{r}\frac{\partial}{\partial r}(ru_p) + \frac{\partial w_p}{\partial z} = 0. \tag{26}$$

Combining (23) and (24) yields:

$$u_p = \frac{-N}{1+4N^2}\frac{\partial P_p}{\partial r}, \tag{27}$$

$$v_p = \frac{2N^2}{1+4N^2}\frac{\partial P_p}{\partial r}. \tag{28}$$

Using (B.C. 1), (27) and (13*a*), we derive:

$$u_p = \frac{-N}{1+4N^2}\frac{\partial P}{\partial r} = \frac{-N}{1+4N^2}(2v_{I0}) = \frac{-2N}{1+4N^2}rV_{I0} \tag{29}$$

and, from (B.C. 2), (29) and (20)

$$u = u_{I0} + \overline{u}_0|_{z=-1} = rA = u_p = \frac{-2N}{1+4N^2}rV_{I0}.$$

Thus,

$$A = \frac{-2N}{1+4N^2}V_{I0}. \tag{30}$$

Also (B.C. 3), (24), (29) and (21) give

$$v = v_{I0} + \overline{v}_0|_{z=-1} = rV_{I0} + rB = -2Nu_p = \frac{4N^2}{1+4N^2}rV_{I0}.$$

Thus,

$$B = -\left(1 - \frac{4N^2}{1+4N^2}\right)V_{I0}. \tag{31}$$

Using (29) in (26), we find

$$\frac{\partial w_p}{\partial z} = \frac{4N}{1+4N^2} V_{I0}. \tag{32}$$

Integrating (32) and using (B.C. 5) yields

$$w_p = \frac{4N}{1+4N^2} V_{I0} \left(z+1+\frac{h}{L}\right). \tag{33}$$

From (B.C. 4), $w = w_{I0} + \overline{w}_0 + E^{\frac{1}{2}}(w_{I1} + \overline{w}_1)_{z=-1} = w_p|_{z=-1}$,

where w_{I0} and $\overline{w}_0$ vanish. Using (19), (22) and (33),

$$E^{\frac{1}{2}} \left(-\frac{\partial V_{I0}}{\partial \tau} + A + B\right) = \frac{4N}{1+4N^2} \frac{h}{L} V_{I0}.$$

Substituting for A and B from (30) and (31),

$$\frac{\partial V_{I0}}{\partial \tau} + \frac{1}{1+4N^2}\left[\frac{4N}{E^{\frac{1}{2}}} \frac{h}{L} + 2N + 1\right] V_{I0} = 0. \tag{34}$$

Solving (34) using the initial condition that $V_{I0} = -1$ at $\tau = 0$ yields

$$V_{I0} = -\exp\left(-\frac{1}{1+4N^2}\left[\frac{4N}{E^{\frac{1}{2}}} \frac{h}{L} + 2N + 1\right]\tau\right). \tag{35}$$

In dimensional terms,

$$v_{I0} = -r\Delta\Omega e^{-t/T}, \tag{36}$$

where T is defined as the spin-up time,

$$T = \frac{1}{\Omega}\left[\frac{1+4N^2}{(4Nh/L) + 2NE^{\frac{1}{2}} + E^{\frac{1}{2}}}\right]. \tag{37}$$

The effect of the permeable medium is to decrease the spin-up time as compared with ordinary Ekman spin-up. The permeable medium acts somewhat as a centrifugal pump, sucking fluid from the interior down into the medium and forcing it up the sides of the container. This suction is in addition to the Ekman suction, which is still present.

In the experiment described in §3, it was more convenient to use a rigid surface at the top boundary, $z = 0$, and the theory must be modified accordingly.

From (37), we can see that if the spin-up time due only to the Ekman layer (T_ν) is characterized by $\Omega^{-1}E^{-\frac{1}{2}}$, and the spin-up time due only to the permeable medium (T_p) is characterized by $[\Omega((4Nh)/L) + 2NE^{\frac{1}{2}})]^{-1}$ (neglecting the N^2 term which is negligible in practice), then the total spin-up time T can be found by adding T_ν and T_p as if they were parallel resistances:

$$\frac{1}{T} = \frac{1}{T_p} + \frac{1}{T_\nu}. \tag{38}$$

It can easily be shown that the effect of the Ekman layer at the rigid top can be taken care of in similar fashion by adding in parallel the spin-up time associated with it (same as T_ν). Thus for a cylinder of height L with a permeable medium of height h at the bottom and a rigid top,

$$T = \frac{1}{\Omega}\left[\frac{1}{(4Nh/L) + 2NE^{\frac{1}{2}} + 2E^{\frac{1}{2}}}\right]. \tag{39}$$

3. The experimental arrangement and the method of observation

The turntable that was used for the experiments can be rotated at a uniform angular velocity accurate to about 0·1 %. We used a tank with diameter $D = 18{\cdot}7$ cm with a rigid top. For four of the runs, the depth of the fluid L was 10·45 cm, and the height of the permeable medium h was 1·45 cm. For the last two runs, we had $L = 18{\cdot}60$ cm and $h = 1{\cdot}75$ cm. We had tried various types of permeable materials and finally settled on close-packed glass spheres of radius $R = 0{\cdot}4$ cm, because the permeability could be calculated accurately, and the results could be reproduced with ease. The theoretical equation of Brinkman (Scheidegger 1960) for the permeability of spheres packed with a given porosity is

$$k = \frac{R^2}{18}\left[3 + \frac{4}{1-P} - 3\left(\frac{8}{1-P} - 3\right)^{\frac{1}{2}}\right], \tag{40}$$

where P is the porosity. The spheres were packed as close as possible to ensure that the porosity was the known minimum of 0·259. Thus, for our experiments, $k = 0{\cdot}476 \times 10^{-4}$ cm^2. For the kinematic viscosity of water ν we used $0{\cdot}96 \times 10^{-2}$ cm^2/s.

For observing the flows we used a method described by Baker (1966). A pH indicator solution, thymol blue, is used as the fluid. The indicator, blue when basic and yellow when acidic, is titrated to the point where it is very slightly acidic. Conducting wires are stretched across the diameter of the cylinder at different heights, and are connected to a d.c. source. When the wires are pulsed, fluid around the positive wire takes on a blue colour, because the solution becomes locally basic. The blue line forms a neutrally buoyant marker.

The sequence of photographs in figure 2, plate 1, shows this blue line viewed from above as the fluid is spun up for a cylinder with solid boundaries.

Experimental results can be compared to theory by measuring ϕ, the angle between the wire and the line, as a function of time. This can be done by taking sequences of pictures, as shown in figure 2, plate 1, from a camera mounted on the turntable vertically above the cylinder. The theoretical relationship between ϕ and t can be found by integrating (36), which can be written as

$$v = -r\frac{d\phi}{dt}. \tag{41}$$

Integrating the above, and using the condition that $\phi = 0$ at $t = 0$, we have

$$\phi = T\Delta\Omega(1 - e^{-t/T}), \tag{42}$$

where, for a free surface or a rigid top configuration, we use (37) or (39), respectively, for the spin-up time. For $t \to \infty$, ϕ will reach a final value ϕ_f, given by

$$\phi_f = T\Delta\Omega. \tag{43}$$

4. Experimental results and comparison with theory

In practice, we sometimes observed deviations from a straight line for the measurement of ϕ. This indicated that different portions of the interior of the

fluid were spinning up with slightly different rates. Figure 3, plate 2, shows a typical line. The deviation from an exact straight line is probably due to irregularities in the permeable medium, since repeated experiments with a single packing of glass balls reproduced the irregularities in the same locations. An average value of ϕ could be easily determined.

The average values of ϕ, determined from experiment, were compared with theory. Figures 4(a)–(f) show this comparison. In these figures ϕ is plotted as a function of $e^{-t/T}$ where T is the theoretical value for the spin-up time calculated from (39). T_ν and T_p are defined† in the paragraph preceding (38). The ratio T_p/T_ν^1 is a measure of the relative influences of the Ekman boundary layer and the permeable medium. The former tends to dominate as the ratio is increased from unity, the latter dominates as the ratio is decreased from unity. This ratio, calculated for our experimental conditions, is shown in table 1.

Run	L (cm)	h (cm)	Ω (rad/s)	$\Delta\Omega/\Omega$	T_p/T_ν	T (sec)
1	10·45	1·45	1·10	0·0132	5·78	43·5
2	10·45	1·45	2·73	0·0133	1·47	19·3
3	10·45	1·45	3·74	0·0132	0·91	13·1
4	10·45	1·45	4·85	0·0092	0·61	9·2
5	18·60	1·75	6·48	0·0304	0·34	9·6
6	18·60	1·75	8·15	0·0163	0·23	6·4

TABLE 1. Values of parameters for experiments shown in figures 4–9.

The comparison of experiment with theory is quite satisfactory, being within 8 % of agreement for every case. The difference between theory and experiment is greatest ($\sim 8\,\%$) for the slowest rotation rate ($\Omega = 1{\cdot}10$ rad/s) where the Ekman layers dominate, and the fastest rate (8·15 rad/s) where the permeable medium dominates. For the slow case, the spin-up time is about 40 sec, which means the time required to reach 99 % of the final angle is about $3\frac{1}{2}$ min. Thermal effects, which are described below, are maximum for this case. Also, since the effects of the Ekman layer dominate, the irregularities of the interface between the permeable medium and the free fluid are also maximum. For the very fast case there seems to be much more unevenness in the line, as shown in figure 8 in §5. As described there, there are unusual effects in the side wall boundary layer, which may have something to do with this unevenness in the interior. With the unevenness it is difficult to determine the position of the dye line very accurately.

The main sources of experimental error are: (i) slow thermal flows generated by the temperature difference between the experimental fluid and the air in the laboratory; (ii) viscous drag of the wire on the flow past the wire and (iii) unevenness in packing of the glass spheres and the consequent (horizontal) spatial variation in the permeability.

Thermal effects were minimized by setting up the experimental arrangement several hours before the actual runs, and allowing the system to come to thermal

† When a rigid top is used T_ν is given by $\frac{1}{2}\Omega^{-1}E^{-\frac{1}{2}}$.

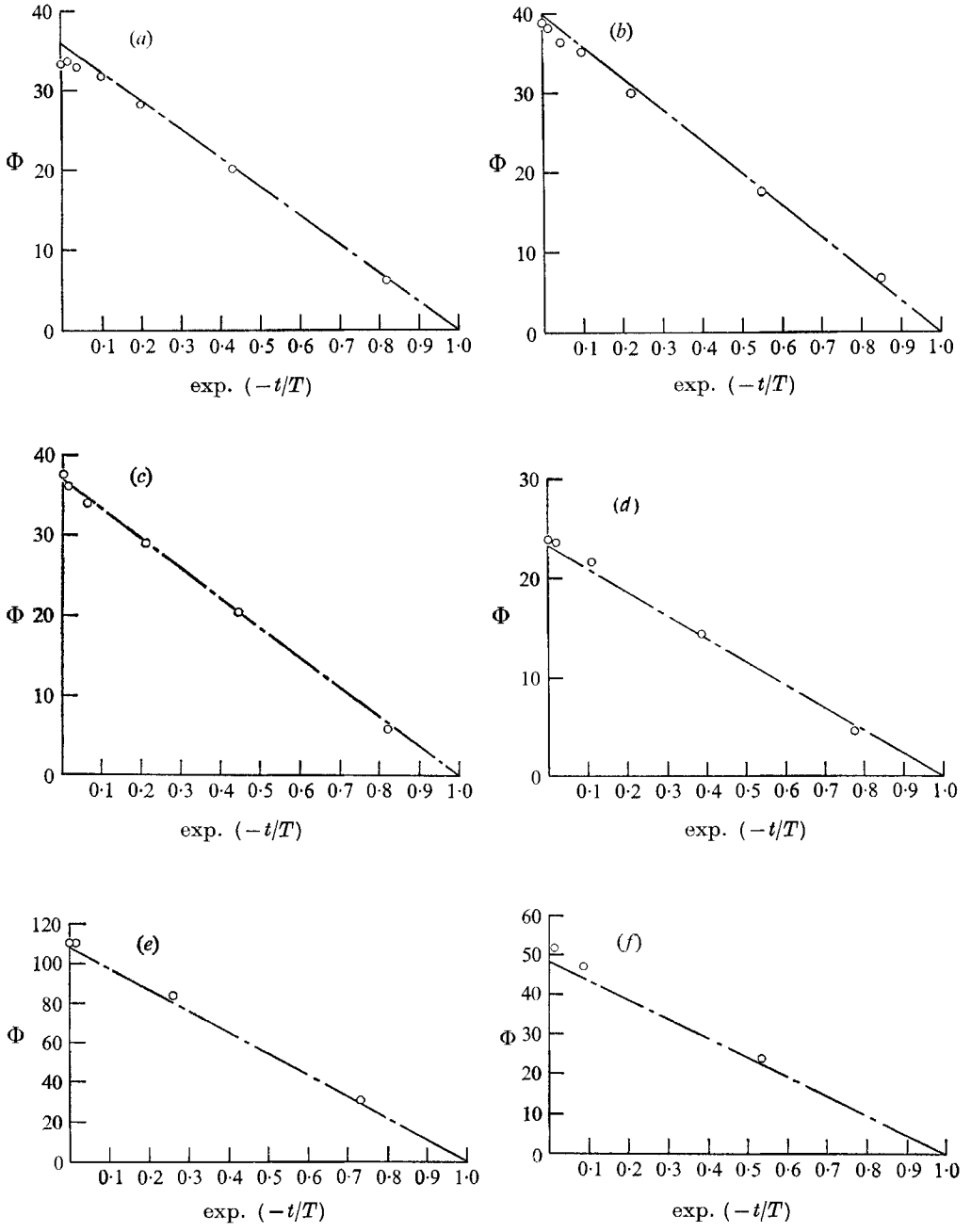

FIGURE 4. A comparison of theory (— · —) and experimental data (○) for: (*a*) run 1 (Ω = 1·10 rad/s, $\Delta\Omega/\Omega$ = 0·0132, T = 43·5 s); (*b*) run 2 (2·73 rad/s, 0·0133, 19·3 s); (*c*) run 3 (3·74 rad/s, 0·0132, 13·1 s); (*d*) run 4 (4·85 rad/s, 0·0092, 9·16 s); (*e*) run 5 (6·48 rad/s; 0·0304, 9·61 s, and L = 18·6 cm, h = 1·75); (*f*) run 6 (8·15 rad/s, 0·0163, 6·36 s, 18·6 cm 1·75).

equilibrium with the room temperature. Also, the water that was used was stored in a large bottle in the laboratory, and consequently was essentially in thermal equilibrium at the time of use. However, the air temperature fluctuated by a degree or two during the course of the day, and the generated temperature difference created slow thermal flows, which could be observed when the fluid was supposed to be in solid-body rotation. A better arrangement would be to use a tank with a false wall for insulation, but this was not done, as the thermal effects were not really serious enough to distort the results appreciably.

The viscous drag of the wire on the fluid, and most particularly on the dyed line, created an apparently faster spin-up (by about 3 %) near the centre of the tank. This relatively small error can be eliminated by removing the wire after the line is generated.

The unevenness in the packing of the glass spheres cannot really be eliminated completely. Considerable care was used in packing the spheres to minimize the variation in permeability. In any event, an average permeability can be determined, and seems to provide enough accuracy for the spin-up time.

5. Experimental observations of the side-wall boundary layer

Howard (1969) analyzed the side-wall boundary layer theoretically. In his analysis he assumed $\delta = h/L$, T_p/T_ν and N all to be small, making the calculation as an expansion in powers of δ. A significant parameter in the development is $\beta = (\nu T/h^2)^{\frac{1}{2}}$ a measure of the spin-up time relative to the diffusion time based on the scale h. Howard made numerical calculations for large and small β.

The case with small β is more interesting physically since Howard predicts a region near the side boundary, of thickness $h\beta^{\frac{2}{3}}$, in which the fluid spins down. Here, the azimuthal velocity of the fluid lags behind that of the fluid closer to the centre. Howard assumed that the side-wall boundary layer generated by the permeable medium is much thicker than the $E^{\frac{1}{4}}$ layer. It was not possible for us to achieve his conditions when we used water, because the viscosity of water is too large to enable one to juggle the parameters appropriately. In the runs that we made Howard's boundary layer was always thinner than the $E^{\frac{1}{4}}$ layer at the end of a spin-up time. However, the layer of thickness $h\beta^{\frac{2}{3}}$ is generated essentially instantaneously, whereas the viscous diffusion layer achieves the thickness $E^{\frac{1}{4}}$ at the end of a spin-up time. Hence, the qualitative effects of Howard's theory could be observed, but the flow pattern was affected by the $E^{\frac{1}{4}}$ layer during the course of the run, and we were unable to reproduce his quantitative results.

We first observed the boundary layer from the side. There exists a point along any radius from the interior to the side wall, where the final vertical displacement of the fluid particles after the spin-up process has been completed is zero. We shall refer to this point as the zero point. The radial distance of this point from the wall can be theoretically calculated for small β from Howard's theory. We sought to measure this distance experimentally.

To measure the radial distance of interest, a camera was fixed to the turntable, so that the tank was viewed from the side. The circular cylindrical tank was placed inside a square-bottomed tank filled with water. One of the flat sides

of this tank was placed perpendicular to the line of sight of the camera, which was fixed at a distance of about 60 cm from the side. The optical distortion of the sides of the circular tank was thereby essentially eliminated.

The wire was placed at a certain angle (looking down from the vertical) with respect to the line of sight of the camera. The fluid was spun up an amount such that the part of the marker line containing the zero point ended up perpendicular to the line of sight of the camera. This goal could only be achieved approximately.

We looked at cases in which the azimuthal displacement of the point of zero vertical displacement was 45° and 90°. Two runs were made for each angle. Figure 5, plate 3, shows the marker line after a 90° displacement. (The conditions for this case are summarized in table 2 as the conditions for figure 5.) The dashed line represents the horizontal plane containing the wire, which generated the marker. The figure shows the upward displacement near the wall. The line seems to curve back on itself because of our viewpoint. Of primary interest, however, is the distance from the wall to the zero point.

Figure	L (cm)	h (cm)	Ω (rad/s)	$\Delta\Omega/\Omega$	T_ν	T_p (s)	T (s)	$h\beta^{\frac{2}{3}}$ (cm)	$LE^{\frac{1}{4}}$ (cm)
5	16·50	2·95	3·02	0·0244	91·2	18·1	15·8	0·76	0·97
6	17·25	1·75	6·37	0·0060	69·8	11·8	10·2	0·56	0·82
7	17·25	1·75	2·78	0·0130	106·0	63·2	39·6	0·87	1·01
8	18·60	1·75	6·48	0·0304	37·9	12·9	9·6	0·54	0·60†

† In this case $L = 18{\cdot}60/2$ cm to evaluate $LE^{\frac{1}{4}}$, because we have a rigid top.

TABLE 2. Values of parameters for experiments shown in figures 5 to 8.

For these cases, the packing of the glass spheres was such that the permeability k had a value of $0{\cdot}80 \times 10^{-4}$ cm^2. This value was obtained by observing the spin-up at several different speeds. With this value for k, and the other conditions given in table 2, the values of the parameters for Howard's theory are $\delta = 0{\cdot}18$, $T_p/T_\nu = 0{\cdot}21$, $N = 2{\cdot}46 \times 10^{-2}$, and $\beta = 0{\cdot}13$.

For an angle of 45° an average radial distance of 1·36 cm, and for 90° an average distance of 1·49 cm was obtained for the two trials. Howard's theory predicts 1·52 cm as the distance between the wall and the zero point for the conditions that we used. The quantitative agreement between theory and experiment is therefore fairly good. It should be pointed out that the $E^{\frac{1}{4}}$ layer, and the $h\beta^{\frac{2}{3}}$ layer, act in the same sense as far as the vertical displacement is concerned.

The second prediction of Howard's theory which we tried to measure experimentally is the backward displacement or lag of the fluid azimuthally in the $h\beta^{\frac{2}{3}}$ layer. Physically, the reason for this lag is clear. The fluid in the permeable medium and near the axis of rotation is thrown outward by the increased centrifugal force due to the larger rotation rate. Because of the spreading of the radial lines, an outward divergence is generated in the permeable medium, and fluid is sucked down from the interior. Near the outer wall, however, the radial flow decreases outward and in a region of thickness $O(h)$ the fluid converges outward.

In the free fluid near the outer wall, there is an upward flow and the magnitude of the inward radial flow decreases toward the wall. The decreased inward radial flow means that particles of fluid acquire a smaller increase in angular velocity than do particles closer to the centre. Hence, fluid in this outer region will appear to lag behind the fluid closer to the centre. In this case, the diffusive effect of the $E^{\frac{1}{4}}$ layer will be to increase the angular velocity of the fluid near the wall. Hence, the viscous $E^{\frac{1}{4}}$ layer will tend to decrease the effect of the essentially inviscid layer of thickness $h\beta^{\frac{2}{3}}$. As long as the latter layer is thicker than the $E^{\frac{1}{4}}$ layer, as it is shortly after the initial instant, the lag should be as Howard has predicted. As the effects of the $E^{\frac{1}{4}}$ layer diffuse into the interior fluid, the effect of the $h\beta^{\frac{2}{3}}$ layer should be decreased.

In our experiments, we were restricted to cases where the $E^{\frac{1}{4}}$ layer was at least as thick as the $h\beta^{\frac{2}{3}}$ layer. Hence, our observations, which were made at the end of the spin-up time, reflected very strong effects of the $E^{\frac{1}{4}}$ layer. As a result, we were able to provide only qualitative confirmation of Howard's predictions.

The qualitative difference in the azimuthal velocities of two flows, of which one satisfies Howard's assumptions and the other does not, is shown by figure 6, plate 4, and figure 7, plate 5. The experimental conditions for these two flows are given in table 2. From these data, we note that for figure 6, $\delta = 0{\cdot}10$, $T_p/T_\nu = 0{\cdot}17$, $\beta = 0{\cdot}18$, i.e. the three parameters for Howard's prediction are considerably less than unity. The dashed line in the figure represents the final angle ϕ_f of the dye line for the interior, as predicted by theory. The backward displacement or lag is evident in the dye line. For figure 7, the parametric values are $\delta = 0{\cdot}10$, $T_p/T_\nu = 0{\cdot}60$, $\beta = 0{\cdot}35$. Hence, both T_p/T_ν and β are considerably larger than in the former case. In figure 7, there is no lag in the azimuthal velocity profile.

For the two cases described above, the top surface was free. By introducing a rigid surface at the top, we can cut down the thickness of the $E^{\frac{1}{4}}$ layer. However, a rigid top also has the disadvantage of increasing the ratio T_p/T_ν. By a suitable juggling of parameters it is possible to optimize the conditions required for the applicability of Howard's theory.

In figure 8, plate 6, we show a large lag in the azimuthal velocity produced in an experiment with parameters given in the last row of table 2. Here $\delta = 0{\cdot}094$, $T_p/T_\nu = 0{\cdot}34$, $\beta = 0{\cdot}17$. The two side-wall boundary layers are comparable in thickness. In addition to the large lag, a small forward displacement is evident radially inward from the lag.

The magnitude of the lags shown in experiments 6 and 8 is about 12% of the interior displacement of the dye line from its original position. According to Howard's theory, the additional lag in the $h\beta^{\frac{2}{3}}$ layer should be about 50% of the displacement of the interior line.

The large quantitative difference between theory and experiment appears to us to be due to the effect of the $E^{\frac{1}{4}}$ layer. However, the qualitative effect of the $h\beta^{\frac{2}{3}}$ layer is evident in figures 6 and 8.

We are indebted to E. A. Spiegel for calling our attention to the need for these experiments. He and L. N. Howard have been most helpful in discussing various

aspects of the problem. The research was supported by the National Science Foundation, grant GA-1416.

REFERENCES

BAKER, D. J. 1966 A technique for the precise measurement of small fluid velocities. *J. Fluid Mech.* **26**, 573–575.

BRETHERTON, F. P. & SPIEGEL, E. A. 1968 The effect of the convection zone on solar spin-down. *Astrophys. J. Letters*, August.

EKMAN, V. W. 1905 On the influence of the earth's rotation on ocean-currents. *Ark. Mat. Astr. Fys.* **2**, 1–52.

GREENSPAN, H. P. 1968 *The Theory of Rotating Fluids*. Cambridge University Press.

GREENSPAN, H. P. & HOWARD, L. N. 1963 On a time dependent motion of a rotating fluid. *J. Fluid Mech.* **17**, 385–404.

HOWARD, L. N. 1969 The effect of side walls on the porous-medium spin-up problem. *Deep-Sea Res. Supplement to* **16**.

SCHEIDEGGER, A. E. 1960 *The Physics of Flow through Porous Media*. University of Toronto Press.

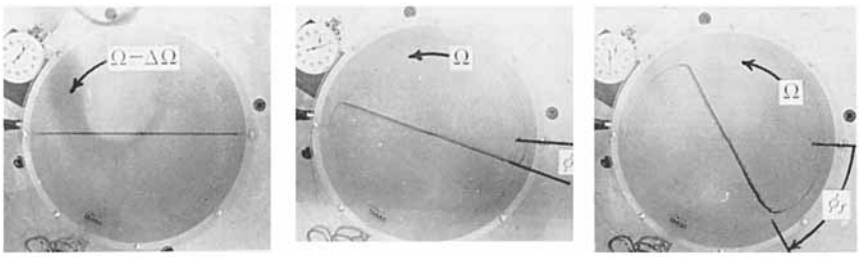

FIGURE 2. The movement of the marker line as the tank is spun up.

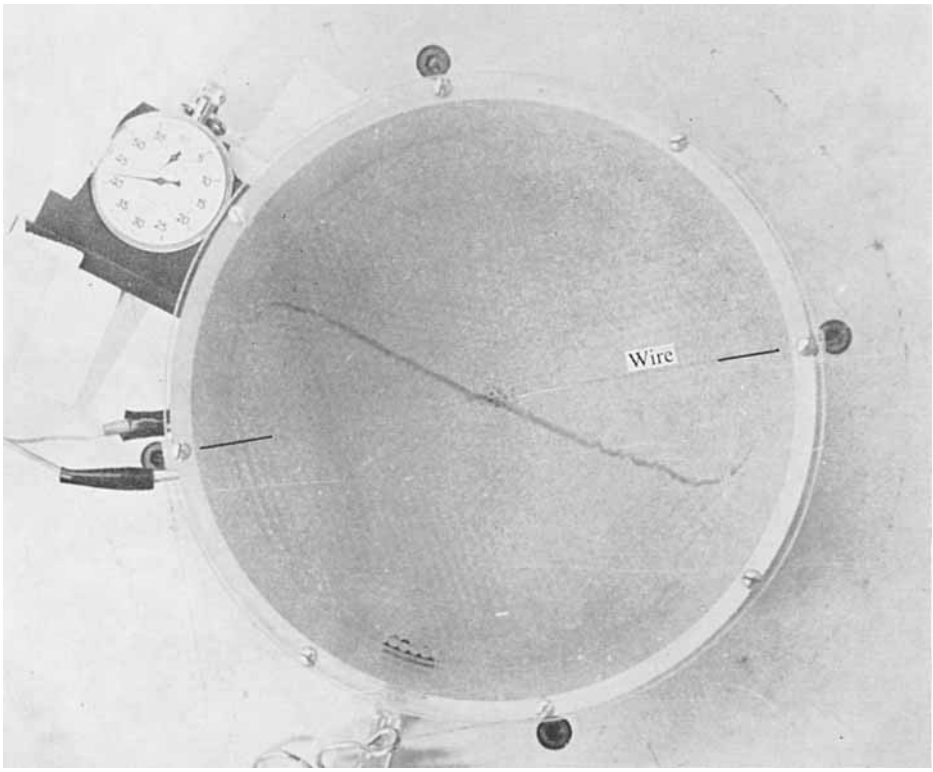

FIGURE 3. A typical marker line after spin-up has been completed.

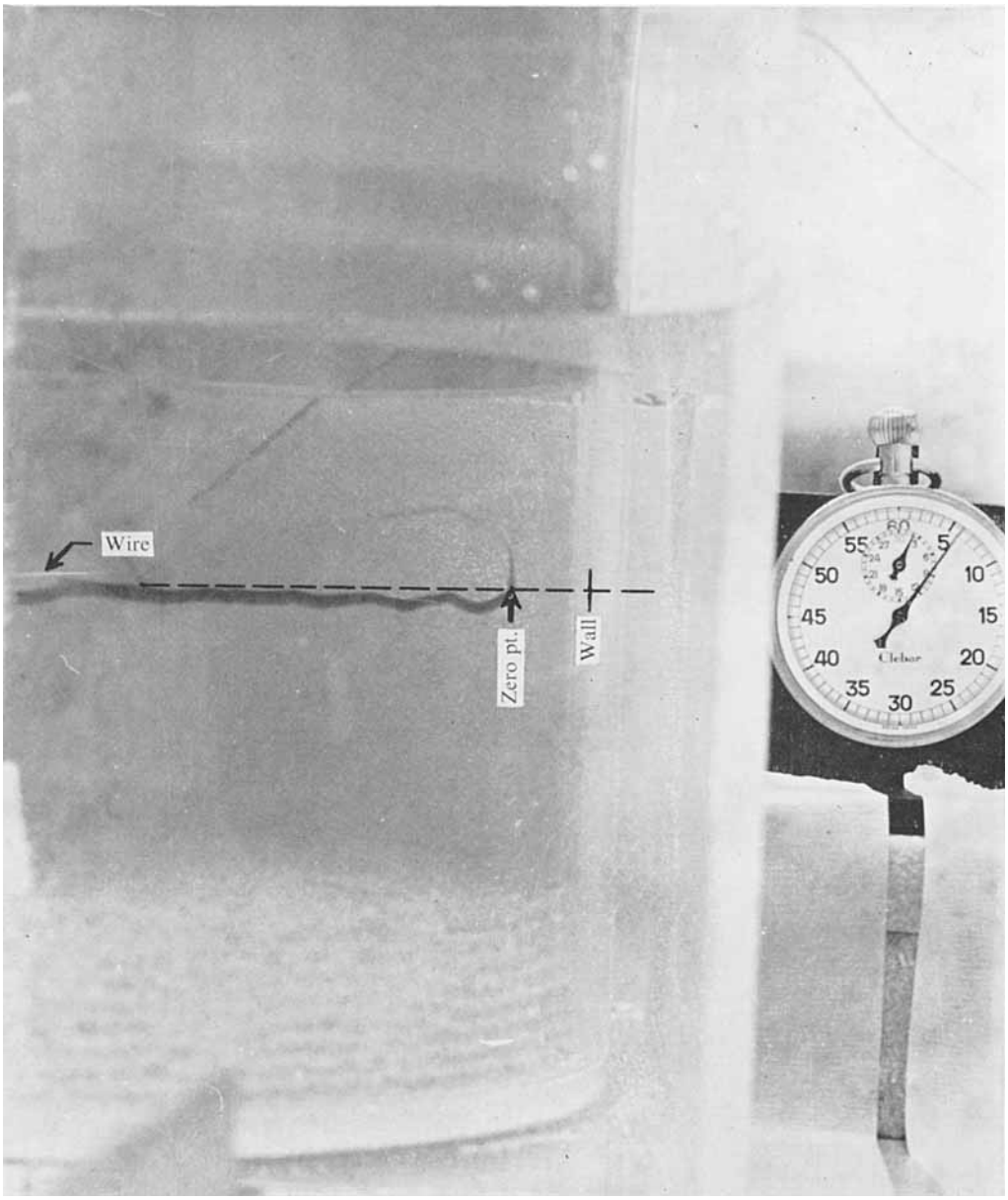

FIGURE 5. Lateral view of the side-wall boundary layer with $\beta = 0{\cdot}13$ and $T_p/T_\nu = 0{\cdot}21$.

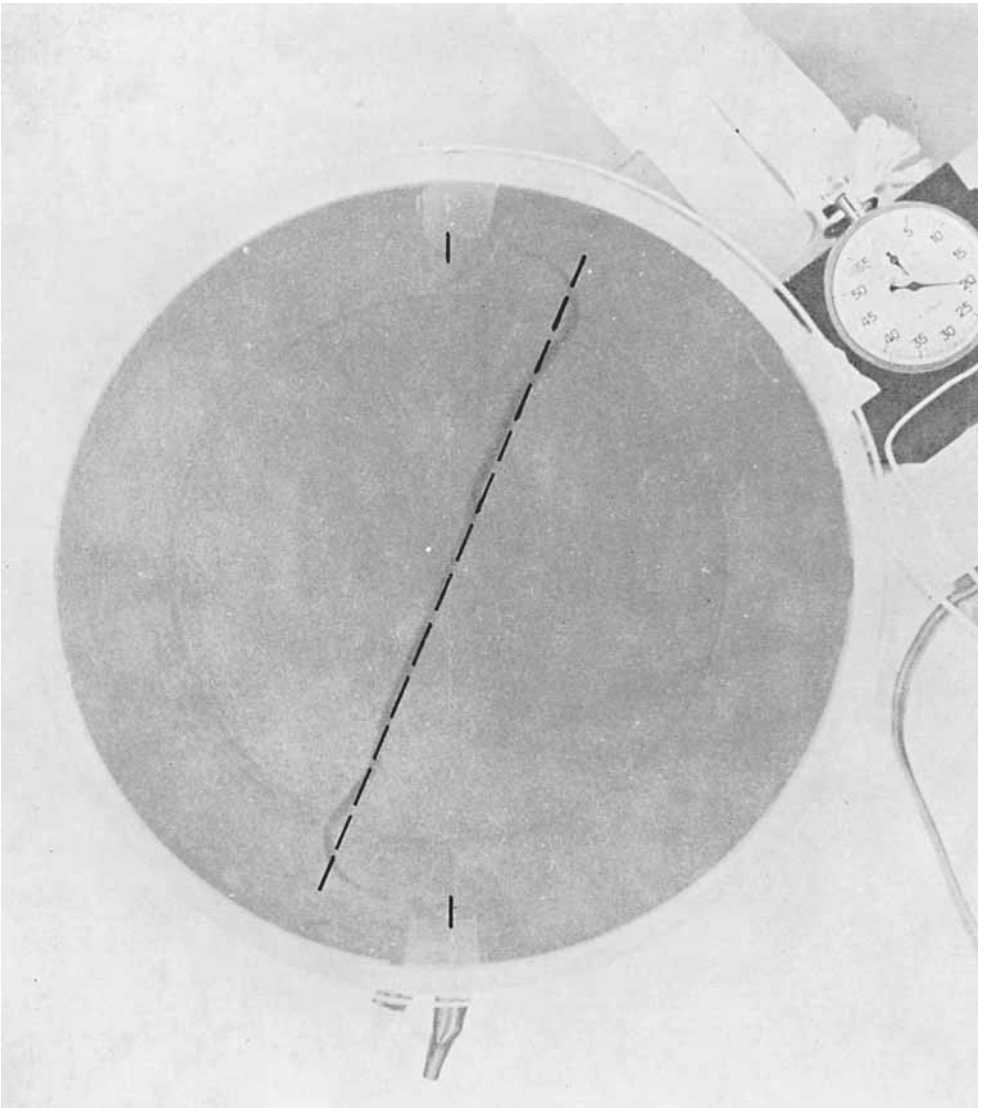

FIGURE 6. Vertical view of the side-wall boundary layer with β and T_p/T_v small ($\beta = 0{\cdot}18$, $T_p/T_v = 0{\cdot}17$).

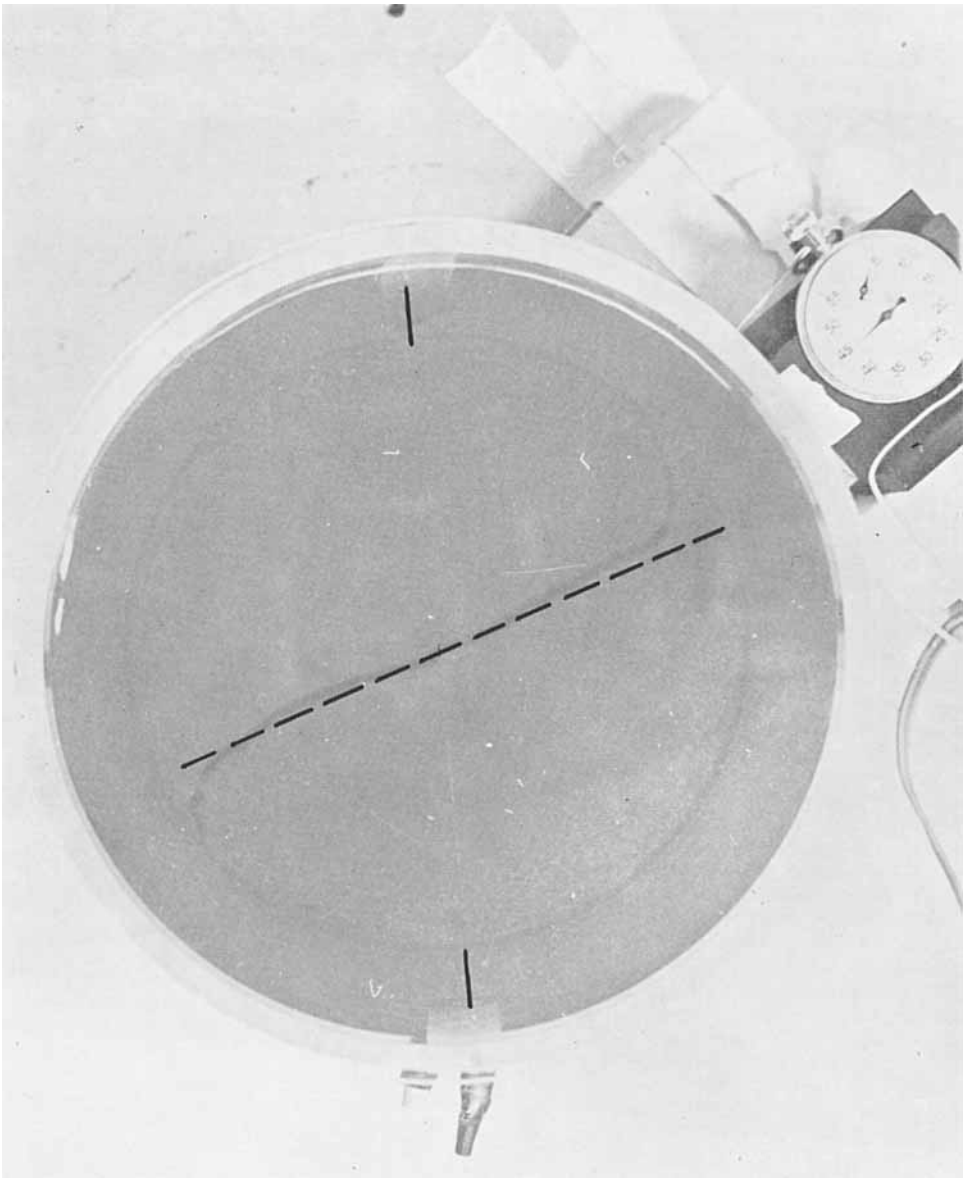

FIGURE 7. Vertical view of the side-wall boundary layer with β and T_p/T_ν not small ($\beta = 0{\cdot}35$, $T_p/T_\nu = 0{\cdot}60$).

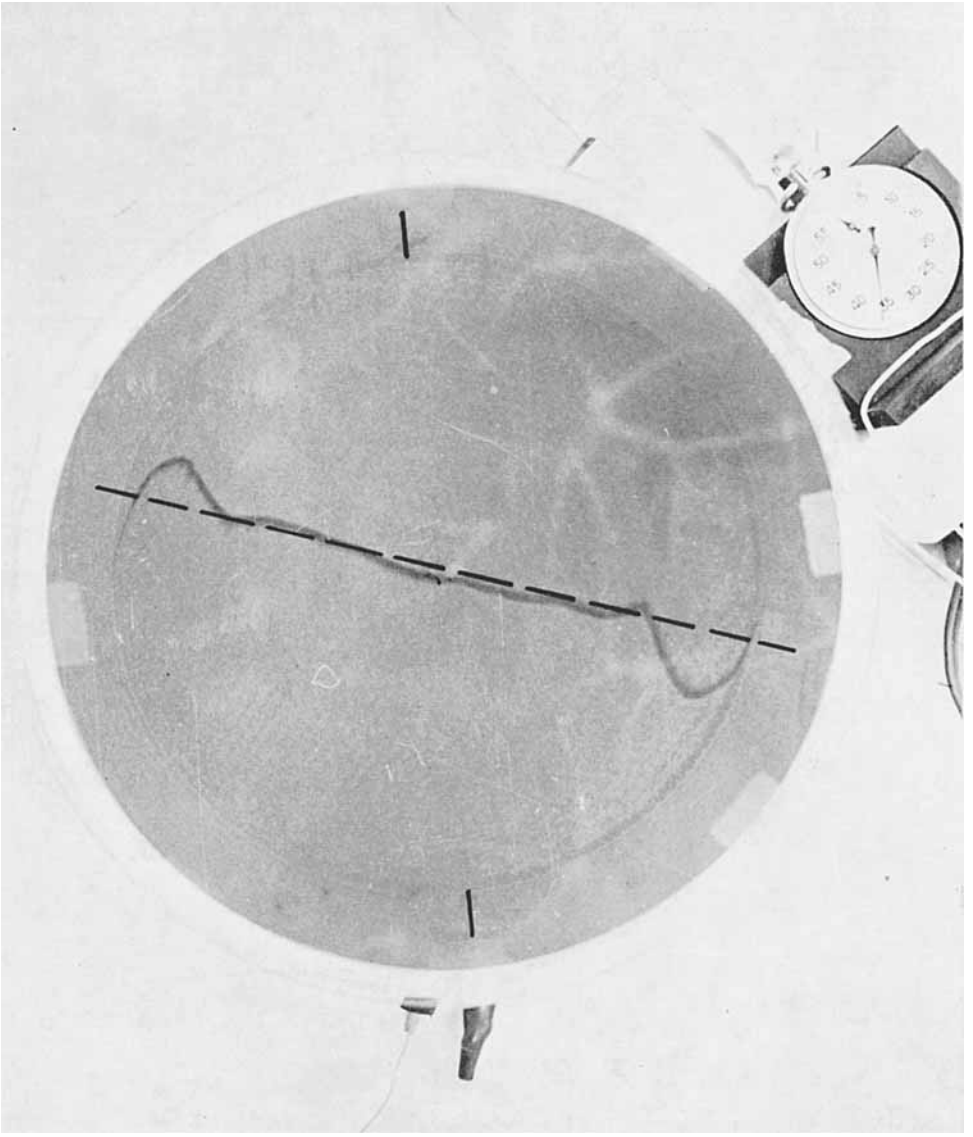

FIGURE 8. Vertical view of the side-wall boundary layer using a rigid top with $\beta = 0{\cdot}17$ and $T_p/T_v = 0{\cdot}34$.